

TABLE 1. Log of Observations

Subfield Name	Field Center (2000) or Offset		Date	$J$ Exposures	$K$ Exposures	Notes
c1a (g0.0-0.8)	$17^h 48^m 16.6^s$	$-29^\circ 21' 37''$	920714	$5 \times 30$ sec	$5 \times (1, 10)$ sec	
c1a2	"	"	"	$5 \times 1$	$5 \times 1$	repeat 1a
c1a3	"	"	920715	$5 \times 1$	$5 \times 1$	repeat 1a
c1b	"	$1' \text{ N}$	920714	$5 \times (1, 30)$	$5 \times (1, 10)$	
c1b2	"	"	"	$5 \times 1$	$5 \times 1$	repeat 1b
c2a (g359.7-0.2)	17 45 24.8	-29 15 48	930706	$5 \times 5; 10 \times 60$	$5 \times (1, 20)$	
c2b	"	$1' \text{ N}$	"	$5 \times (5, 60)$	$5 \times 1$	
c3a (g0.2+0.1)	17 45 06.0	-28 41 18	930707	$5 \times (5, 60)$	$5 \times (1, 3)$	
c3b	"	$1' \text{ N}$	"	$5 \times 5$	$5 \times (1, 3)$	
g0-1.3a	17 50 43.5	-29 36 27	920714	$5 \times (1, 30)$	$5 \times (1, 10)$	
g0-1.3b	$5.1^s \text{ W}$	"	"	$5 \times (1, 30)$	$5 \times (1, 10)$	
g0-1.8a	17 52 42.3	-29 51 45	920714	$5 \times (1, 30)$	$5 \times (1, 10)$	
g0-1.8b	$5^s \text{ W}$	"	"	$5 \times (1, 30)$	$5 \times (1, 10)$	
g0-2.3a	17 54 41.8	-30 06 56	920714	$5 \times (1, 30)$	$5 \times (1, 10)$	
g0-2.3b	$5^s \text{ W}$	"	"	$5 \times (1, 30)$	$5 \times (1, 10)$	
g0-2.8a	17 56 41.9	-30 22 00	920714	$5 \times (1, 30)$	$5 \times (1, 10)$	
g0-2.8a2	"	"	920715	$5 \times 1$	$5 \times 1$	Repeat -2.8a
g0-2.8b	$5.3^s \text{ W}$	"	920714	$5 \times (1, 30)$	$5 \times (1, 10)$	
g0-2.8b2	"	"	920715	$5 \times (1, 10)$	$5 \times (1, 10)$	
g0-2.8c2	"	$70'' \text{ N of b}$	"	$5 \times 1$	$5 \times 1$	g0-2.8c not usable
g0-2.8d2	$0^s \text{ E-W}$	"	"	$5 \times (1, 10)$	$5 \times (1, 10)$	there is no g0-2.8d
g1-1.3a	17 53 03.5	-28 44 50	920715	$5 \times (1, 30)$	$5 \times (1, 10)$	
g2-1.3a	17 55 21.4	-27 53 06	920715	$5 \times (1, 30)$	$5 \times (1, 10)$	
g2-1.3b	$5^s \text{ E}$	"	920718	$5 \times (1, 10)$	$5 \times (1, 10)$	
g3-1.3a	17 57 37.2	-27 01 13	920718	$5 \times (1, 30)$	$5 \times (1, 10)$	
g3-1.3b	$5.2^s \text{ E}$	"	"	$5 \times (1, 10)$	$5 \times (1, 10)$	
g4-1.3a	17 59 51.0	-26 09 14	920718	$5 \times (1, 30)$	$5 \times (1, 10)$	
g4-1.3b	$5.3^s \text{ W}$	"	"	$5 \times (1, 10)$	$5 \times (1, 10)$	
g4-1.3c	"	$70'' \text{ S of b}$	"	$5 \times 1$	$5 \times 1$	
g4-1.3d	$0^s \text{ E-W}$	"	"	$5 \times 1$	$5 \times 1$	

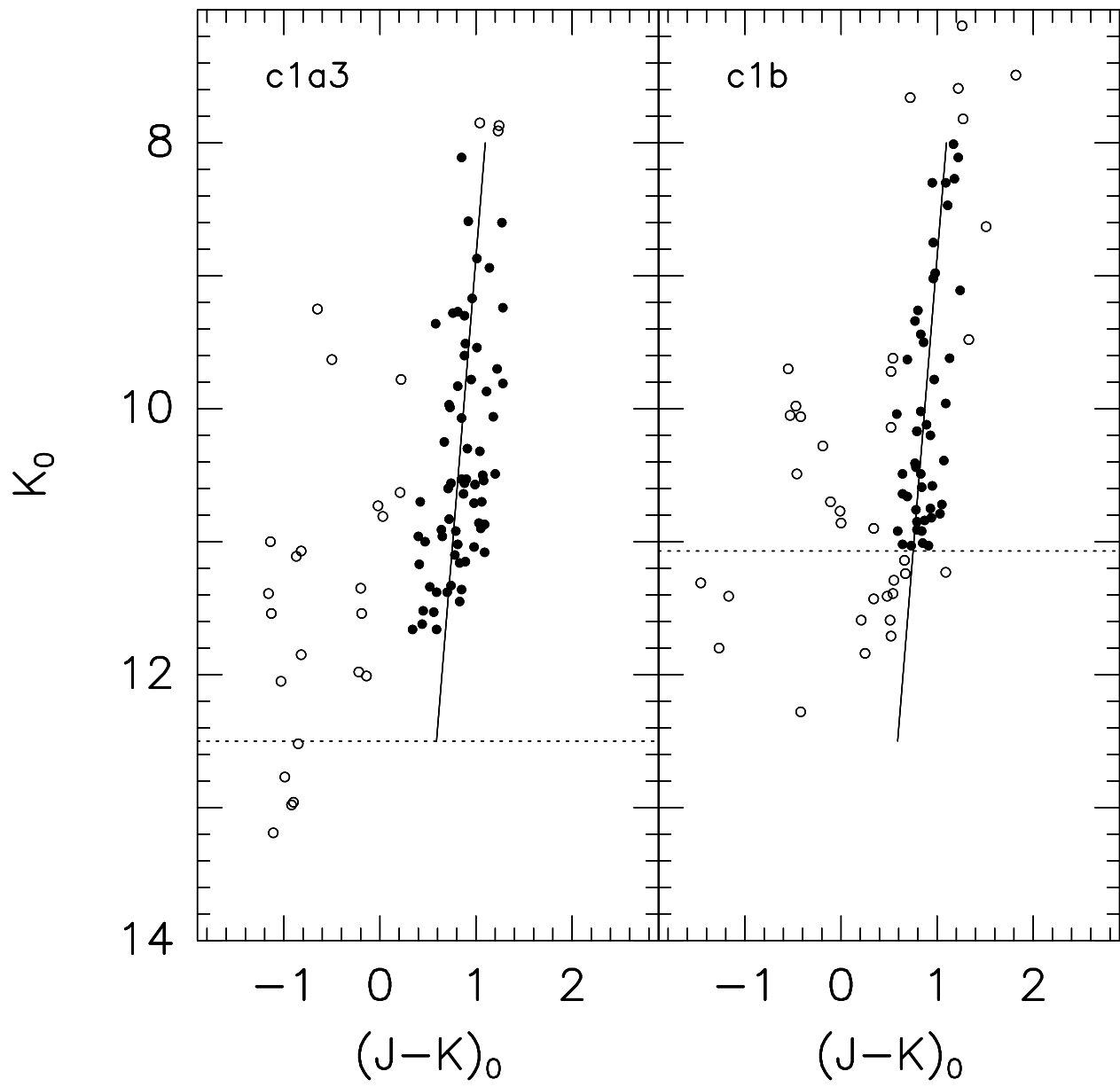


TABLE 2. Reddening

Subfield (1)	$A_K$ (2)	$E(J - K)$ (3)	$\langle A_K \rangle$ (4)	$\sigma$ (5)	Error in Mean (6)	Lower $K$ Limit (7)
c1a	$1.06 \pm 0.07$	$1.71 \pm 0.12$				11.70
c1a2	$1.00 \pm 0.08$	$1.62 \pm 0.12$				11.77
c1a3	$1.05 \pm 0.13$	$1.69 \pm 0.22$				—
c1b	$1.03 \pm 0.09$	$1.67 \pm 0.14$				12.10
c1b2	$1.02 \pm 0.09$	$1.65 \pm 0.15$	1.03	0.02	0.04	11.40
c2a	$2.11 \pm 0.15$	$3.42 \pm 0.24$				11.60
c2b	$2.19 \pm 0.17$	$3.54 \pm 0.28$	2.15	0.06	0.11	11.60
c3a	$1.94 \pm 0.14$	$3.13 \pm 0.23$				11.70
c3b	$1.82 \pm 0.15$	$2.95 \pm 0.24$	1.88	0.08	0.10	—
g0-1.3a	$0.51 \pm 0.06$	$0.82 \pm 0.09$				—
g0-1.3b	$0.47 \pm 0.06$	$0.76 \pm 0.09$	0.49	0.03	0.04	—
g0-1.8a	$0.35 \pm 0.05$	$0.57 \pm 0.07$				—
g0-1.8b	$0.33 \pm 0.05$	$0.53 \pm 0.09$	0.34	0.01	0.04	—
g0-2.3a	$0.27 \pm 0.06$	$0.44 \pm 0.09$				—
g0-2.3b	$0.27 \pm 0.04$	$0.44 \pm 0.07$	0.27	0.00	0.04	—
g0-2.8a	$0.38 \pm 0.05$	$0.62 \pm 0.08$				—
g0-2.8a2	$0.39 \pm 0.07$	$0.63 \pm 0.11$				—
g0-2.8b	$0.38 \pm 0.06$	$0.62 \pm 0.09$				—
g0-2.8b2	$0.41 \pm 0.05$	$0.66 \pm 0.08$				—
g0-2.8c2	$0.43 \pm 0.08$	$0.69 \pm 0.14$				—
g0-2.8d2	$0.41 \pm 0.06$	$0.66 \pm 0.09$	0.40	0.02	0.03	—
g1-1.3a	$0.43 \pm 0.06$	$0.70 \pm 0.10$	0.43	—	0.06	—
g2-1.3a	$0.46 \pm 0.07$	$0.74 \pm 0.12$				—
g2-1.3b	$0.50 \pm 0.07$	$0.81 \pm 0.11$	0.48	0.03	0.05	—
g3-1.3a	$0.56 \pm 0.10$	$0.91 \pm 0.16$				—
g3-1.3b	$0.59 \pm 0.07$	$0.95 \pm 0.11$	0.58	0.02	0.06	—
g4-1.3a	$0.59 \pm 0.10$	$0.95 \pm 0.16$				—
g4-1.3b	$0.55 \pm 0.10$	$0.89 \pm 0.16$				—
g4-1.3c	$0.57 \pm 0.19$	$0.92 \pm 0.30$				—
g4-1.3d	$0.48 \pm 0.20$	$0.78 \pm 0.33$	0.55	0.05	0.08	—

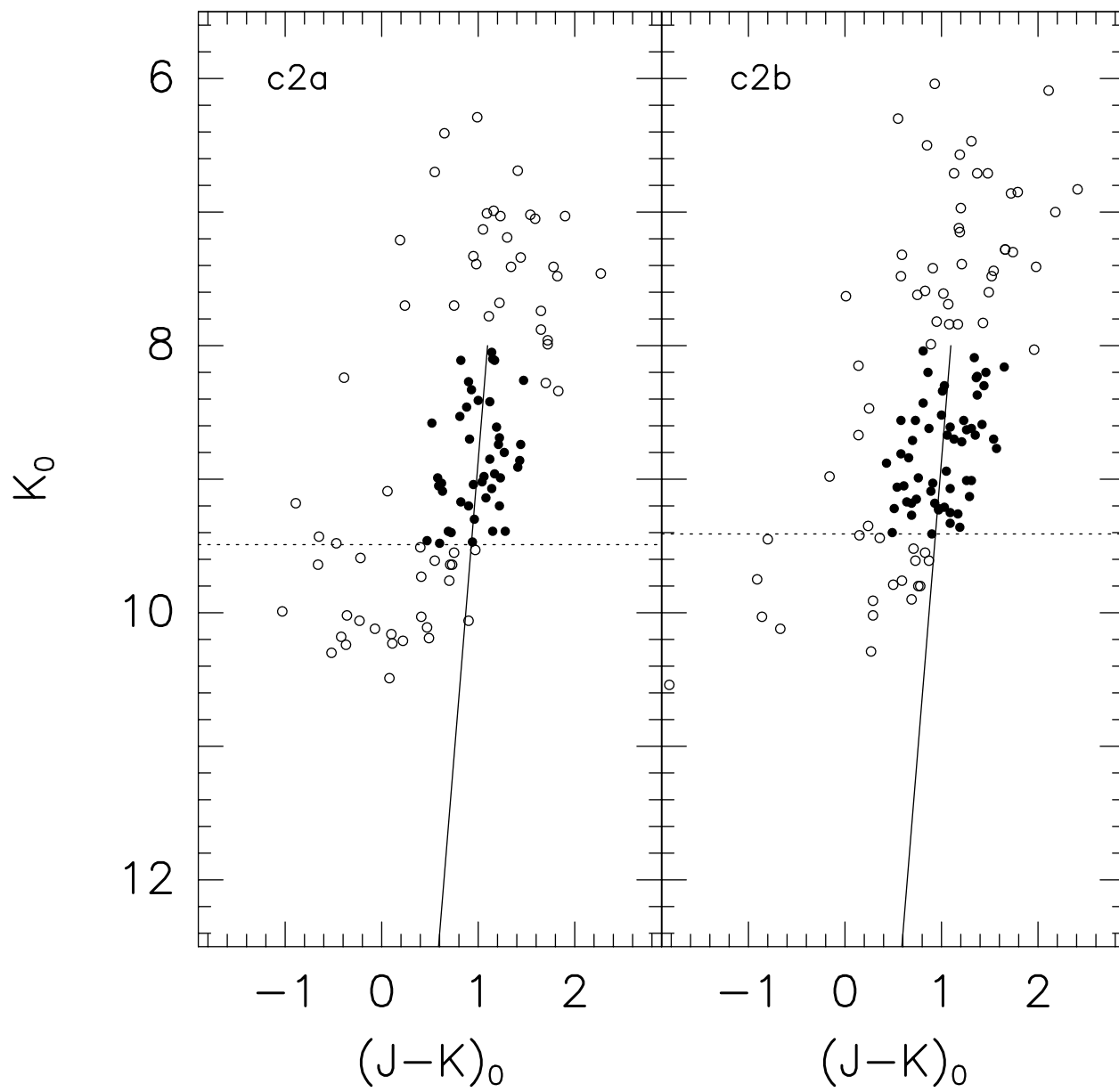


TABLE 3. Giant Branch Slopes and Metallicity

Subfield (1)	N (2)	GB Slope <sup>a</sup> (3)	Intercept (4)	[Fe/H] (5)	$\langle$ [Fe/H] $\rangle$ (6)	$\sigma$ (7)	Error in Mean (8)
c1a3	66	$-0.133 \pm 0.042$	$2.225 \pm 0.310$	$0.12 \pm 0.57$			
c1b	47	$-0.108 \pm 0.022$	$1.970 \pm 0.220$	$-0.22 \pm 0.30$	-0.15	0.24	0.46
g0-1.3a	97	$-0.116 \pm 0.008$	$2.028 \pm 0.092$	$-0.11 \pm 0.11$			
g0-1.3b	93	$-0.112 \pm 0.009$	$2.001 \pm 0.098$	$-0.17 \pm 0.12$	-0.14	0.04	0.12
g0-1.8a	59	$-0.111 \pm 0.010$	$1.992 \pm 0.106$	$-0.18 \pm 0.14$			
g0-1.8b	58	$-0.119 \pm 0.011$	$2.073 \pm 0.129$	$-0.07 \pm 0.15$	-0.13	0.08	0.14
g0-2.3a	56	$-0.117 \pm 0.013$	$2.044 \pm 0.149$	$-0.10 \pm 0.18$			
g0-2.3b	37	$-0.092 \pm 0.012$	$1.737 \pm 0.140$	$-0.44 \pm 0.16$	-0.28	0.24	0.17
g0-2.8a2	48	$-0.092 \pm 0.015$	$1.764 \pm 0.176$	$-0.44 \pm 0.20$			
g0-2.8b2	47	$-0.118 \pm 0.013$	$2.067 \pm 0.151$	$-0.09 \pm 0.18$			
g0-2.8c2	50	$-0.096 \pm 0.021$	$1.798 \pm 0.234$	$-0.39 \pm 0.29$			
g0-2.8d2	50	$-0.105 \pm 0.013$	$1.913 \pm 0.148$	$-0.26 \pm 0.18$	-0.26	0.16	0.18
g1-1.3a	82	$-0.100 \pm 0.009$	$1.855 \pm 0.100$	$-0.33 \pm 0.12$	-0.33	—	0.12
g2-1.3a	68	$-0.085 \pm 0.014$	$1.686 \pm 0.158$	$-0.53 \pm 0.19$			
g2-1.3b	67	$-0.112 \pm 0.011$	$2.001 \pm 0.123$	$-0.17 \pm 0.15$	-0.31	0.26	0.17
g3-1.3a	65	$-0.117 \pm 0.018$	$2.048 \pm 0.209$	$-0.10 \pm 0.25$			
g3-1.3b	56	$-0.159 \pm 0.016$	$2.519 \pm 0.176$	$0.47 \pm 0.22$	0.22	0.40	0.23
g4-1.3a	62	$-0.097 \pm 0.018$	$1.821 \pm 0.201$	$-0.37 \pm 0.25$			
g4-1.3b	34	$-0.148 \pm 0.020$	$2.406 \pm 0.221$	$0.32 \pm 0.27$	-0.06	0.49	0.18

<sup>a</sup>GB slope  $\equiv \Delta(J - K)/\Delta K$ .

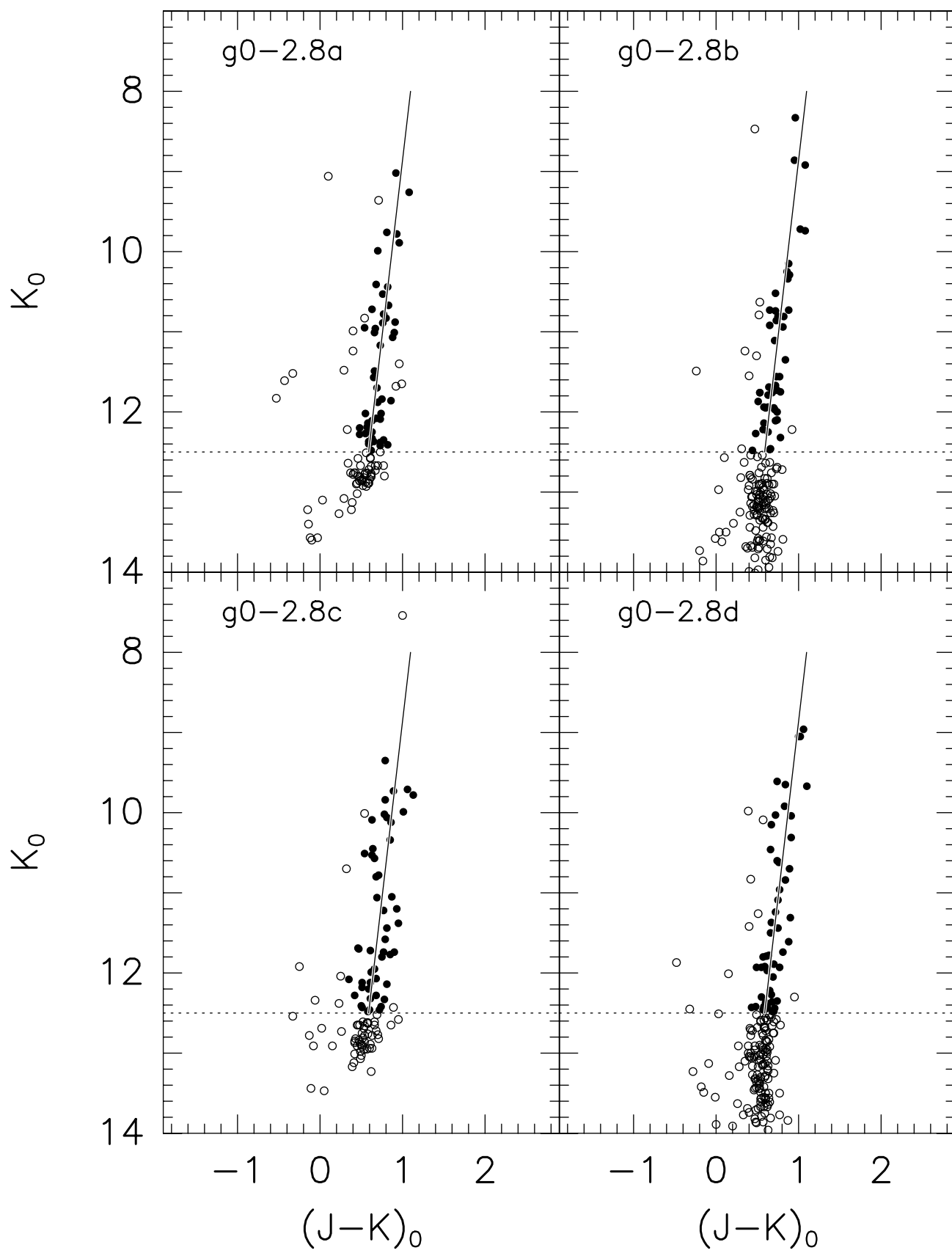






TABLE 4. Metallicity and Latitude

Field	Giant Branch		$\langle[\text{Fe}/\text{H}]\rangle^{\text{b}}$
	b	Slope <sup>a</sup>	
c1	-0.8	—	$-0.15 \pm 0.46$
g013	-1.3	—	$-0.14 \pm 0.12$
g018	-1.8	—	$-0.13 \pm 0.14$
g023	-2.3	—	$-0.28 \pm 0.14$
g028	-2.8	—	$-0.26 \pm 0.18$
Liller 1	-0.20	$-0.135 \pm 0.009$	$0.15 \pm 0.12$
Terzan 2	-2.30	$-0.127 \pm 0.014$	$0.04 \pm 0.19$
BW3	-2.70	$-0.108 \pm 0.013$	$-0.22 \pm 0.18$
BW4	-3.90	$-0.113 \pm 0.005$	$-0.15 \pm 0.07$
BW6	-6.00	$-0.098 \pm 0.007$	$-0.36 \pm 0.10$
BW8	-8.00	$-0.082 \pm 0.010$	$-0.58 \pm 0.14$
BW10	-10.25	$-0.086 \pm 0.014$	$-0.52 \pm 0.19$

<sup>a</sup>Giant branch slopes from Tiede *et al.* (1995)

<sup>b</sup>Tiede *et al.* (1995) values have been recalculated with Equation 3.

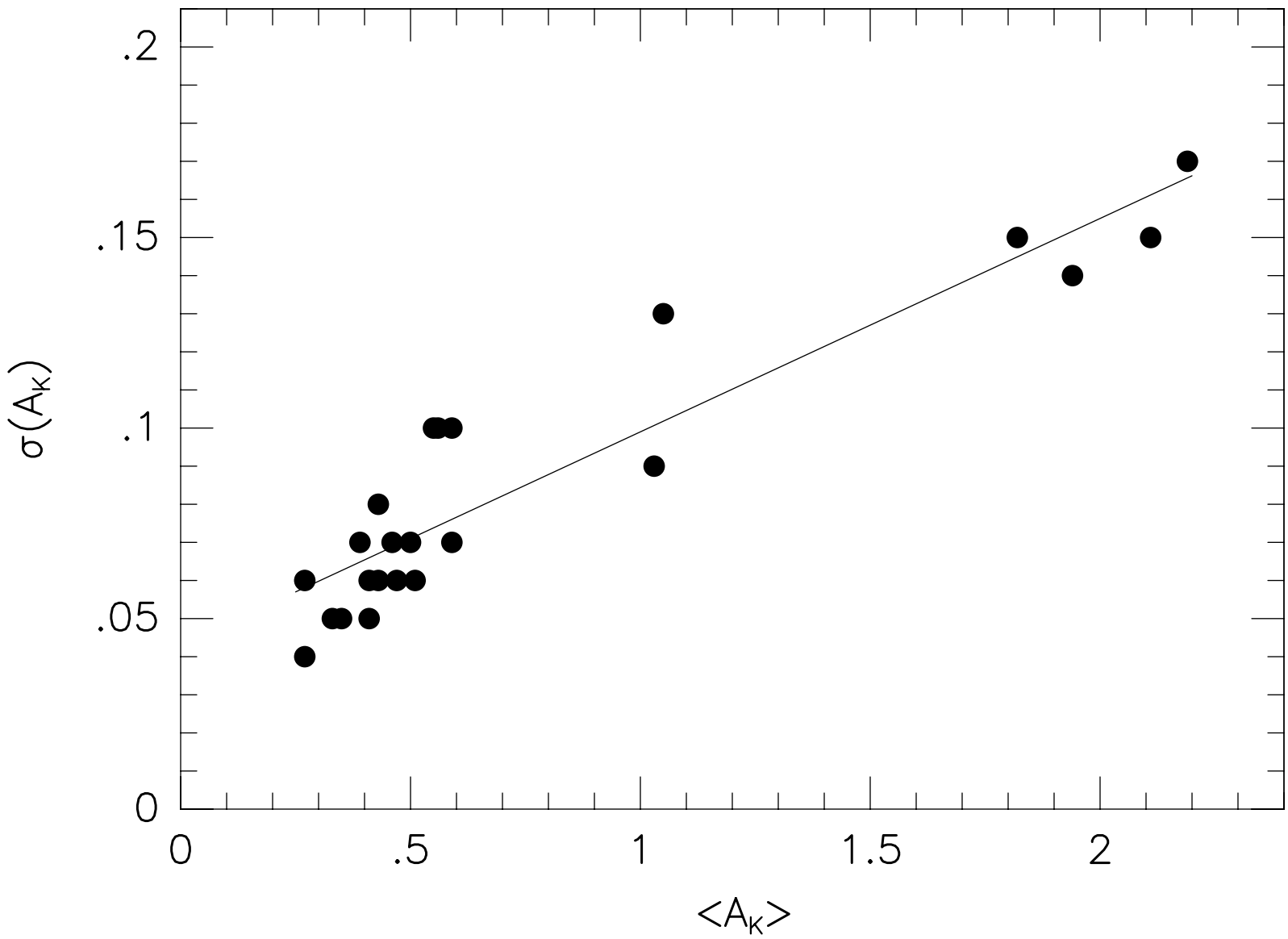


TABLE 5. Minor-Axis Metallicity Gradient

Minor-Axis Gradient (dex/deg)	Intercept <sup>a</sup> (dex)	Data Reference <sup>b</sup>
$-0.060 \pm 0.033$	—	Tiede <i>et al.</i> (1995)
$-0.113 \pm 0.004$	—	Ternstrup <i>et al.</i> (1988)
$-0.038 \pm 0.010$	—	Frogel <i>et al.</i> (1990)
$-0.094 \pm 0.019$	—	Tyson (1991)
$-0.085 \pm 0.033$	$-0.019 \pm 0.066$	this work (inner bulge only)
$-0.064 \pm 0.012$	$+0.034 \pm 0.053$	this work plus Tiede <i>et al.</i> (1995)

<sup>a</sup>This value is the predicted  $\langle[\text{Fe}/\text{H}]\rangle$  value of the bulge population at the Galactic Center.

<sup>b</sup>Source of original data. The gradients based on these data are from Tiede *et al.* (1995), Table 8.

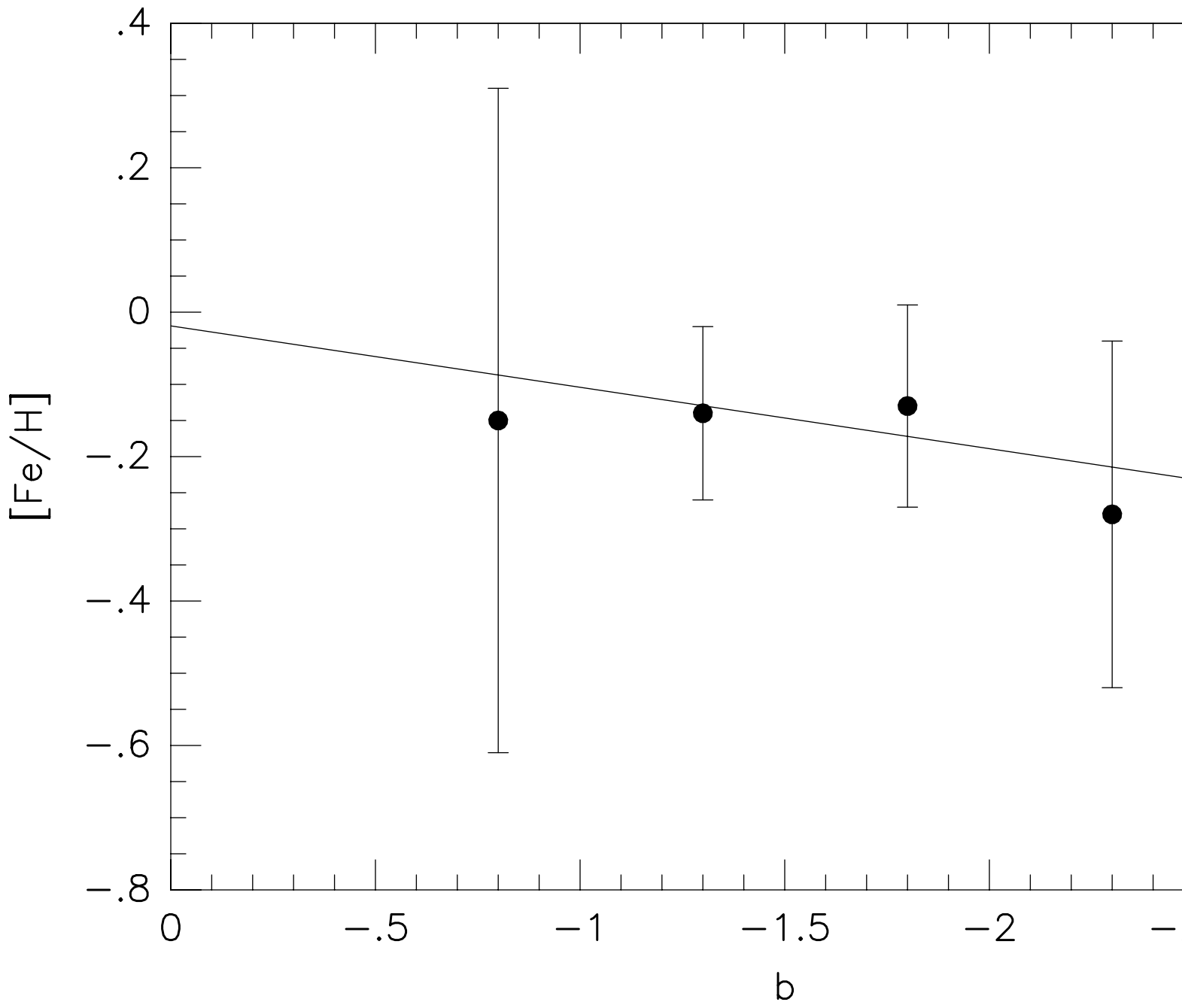
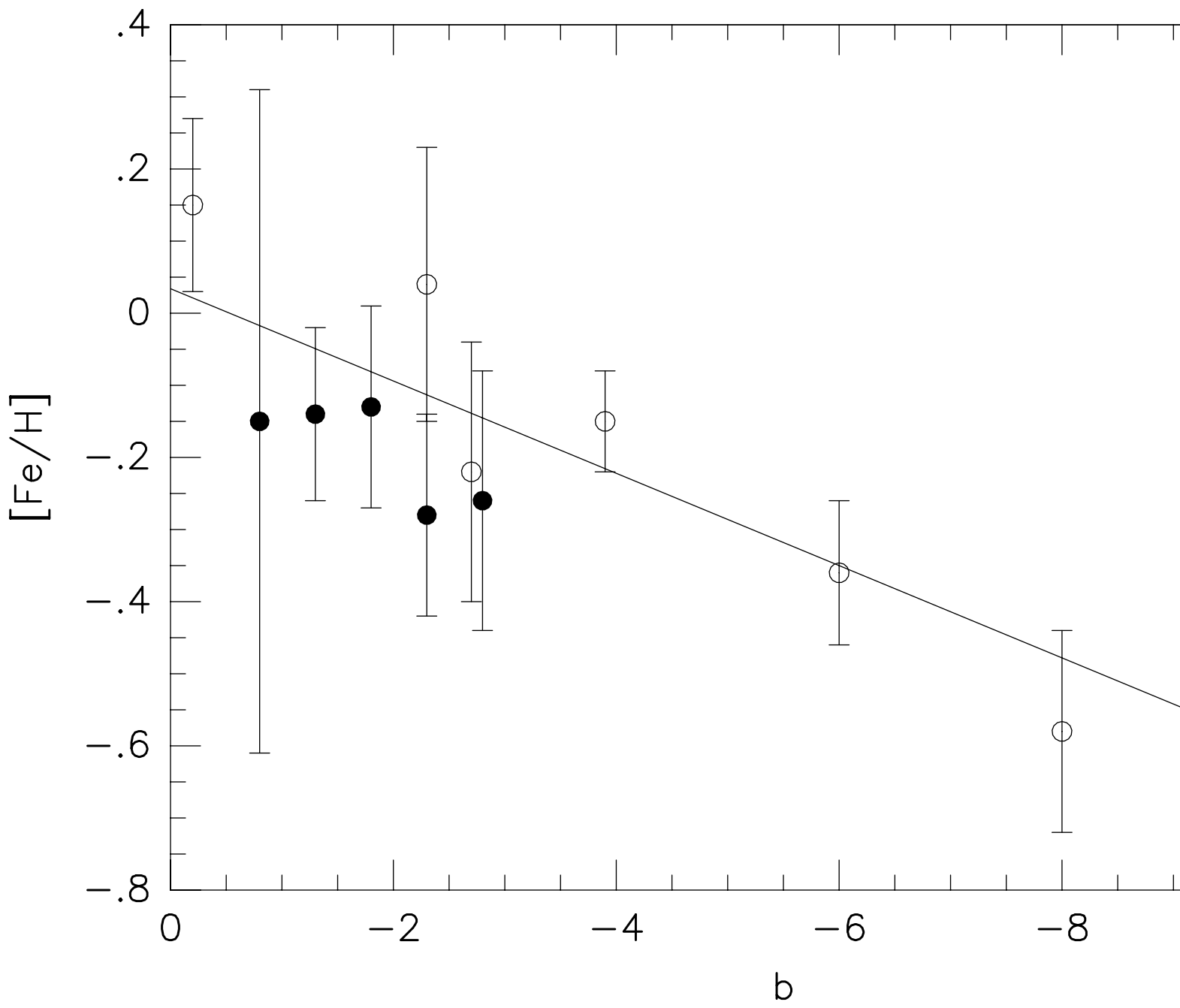
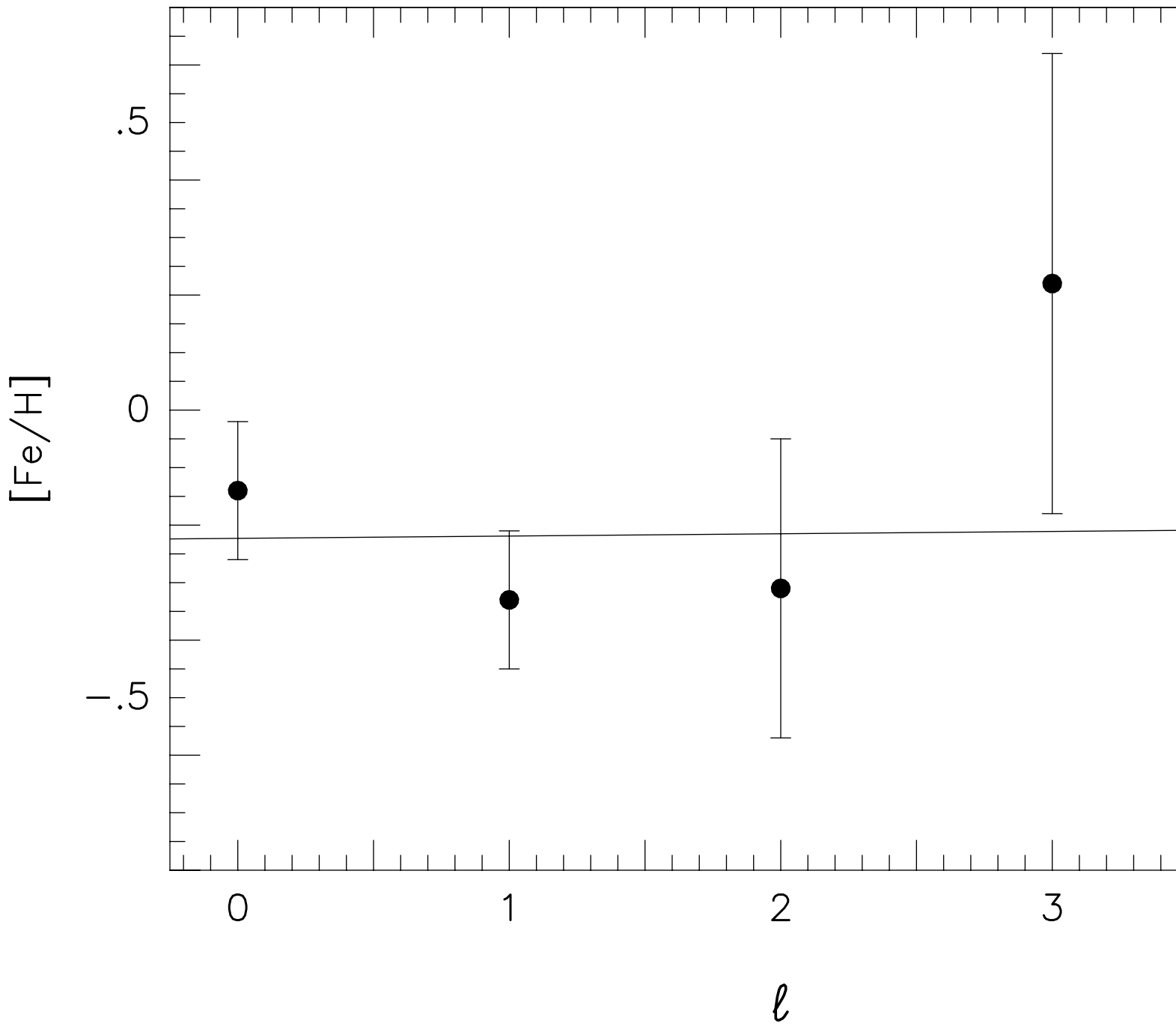
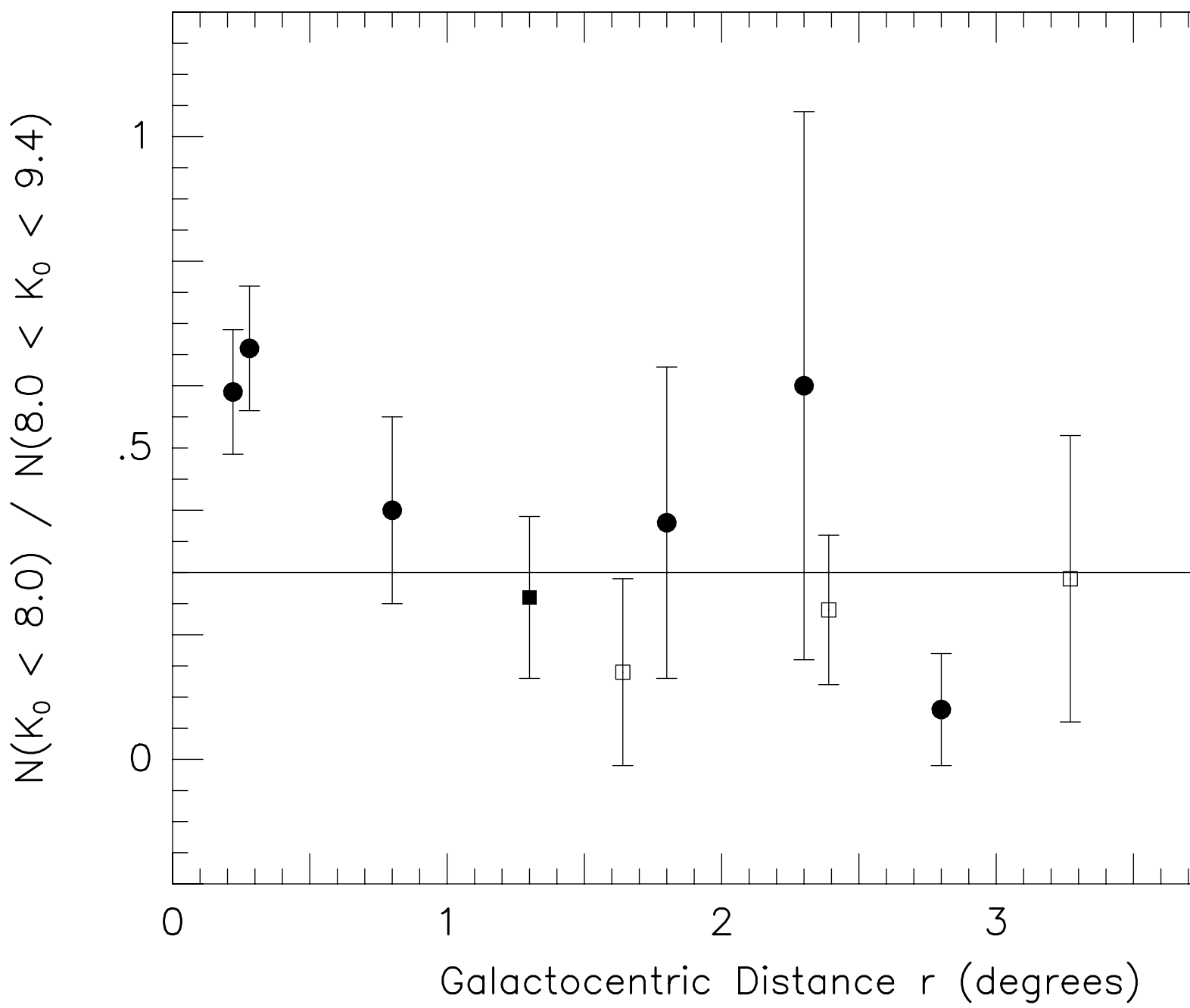


TABLE 6. Ratio of Populations

Field	$(\ell, b)$ (deg)	$r$ (deg)	Number $K_0 < 8.0$	Number $8.0 \leq K_0 \leq 9.4$	Ratio (bright/faint)
c1	( 0.0, -0.8)	0.80	10	25	$0.40 \pm 0.15$
c2	(-0.2, -0.2)	0.28	70	106	$0.66 \pm 0.10$
c3	( 0.2, 0.1)	0.22	50	85	$0.59 \pm 0.10$
g0-1.3	( 0.0, -1.3)	1.30	5	19	$0.26 \pm 0.13$
g0-1.8	( 0.0, -1.8)	1.80	3	8	$0.38 \pm 0.25$
g0-2.3	( 0.0, -2.3)	2.30	3	5	$0.60 \pm 0.44$
g0-2.8	( 0.0, -2.8)	2.80	1	12	$0.08 \pm 0.09$
g1-1.3	( 1.0, -1.3)	1.64	1	7	$0.14 \pm 0.15$
g2-1.3	( 2.0, -1.3)	2.39	5	21	$0.24 \pm 0.12$
g3-1.3	( 3.0, -1.3)	3.27	2	7	$0.29 \pm 0.23$
g4-1.3	( 4.0, -1.3)	4.21	5	11	$0.45 \pm 0.25$









# The Metallicity and Reddening of Stars in the Inner Galactic Bulge

Jay A. Frogel<sup>1</sup>, Glenn P. Tiede<sup>2</sup>, & Leslie E. Kuchinski<sup>3</sup>

Department of Astronomy, The Ohio State University, 174 W. 18th Avenue, Columbus,  
Ohio 43210

Received \_\_\_\_\_; accepted \_\_\_\_\_

In preparation for *The Astronomical Journal*

---

<sup>1</sup>Visiting Research Associate, The Observatories of the Carnegie Institution of Washington.

<sup>2</sup>NOAO, 950 N. Cherry Ave., Tucson, AZ 85719-4933

<sup>3</sup>Current Address: IPAC, California Institute of Technology, Pasadena, CA 91125

## ABSTRACT

We present a preliminary analysis of  $K$ ,  $J - K$  color magnitude diagrams (CMDs) for 7 different positions on or close to the minor axis of the Milky Way at Galactic latitudes between  $+0.1^\circ$  and  $-2.8^\circ$ . From the slopes of the (linear) giant branches in these CMDs we derive a dependence of  $\langle[\text{Fe}/\text{H}]\rangle$  on latitude for  $b$  between  $-0.8^\circ$  and  $-2.8^\circ$  of  $-0.085 \pm 0.033$  dex/degree. When combined with the data from Tiede *et al.* we find for  $-0.8^\circ \leq b \leq -10.3^\circ$  the slope in  $\langle[\text{Fe}/\text{H}]\rangle$  is  $-0.064 \pm 0.012$  dex/degree. An extrapolation to the Galactic Center predicts  $[\text{Fe}/\text{H}] = +0.034 \pm 0.053$  dex.

We also derive *average* values for the extinction in the  $K$  band ( $A_K$ ) of between 2.15 and 0.27 for the inner bulge fields studied, corresponding to average values of  $E(J - K)$  of between 3.46 and 0.44. There is a well defined linear relation between the average extinction for a field and the star-to-star scatter in the extinction for the stars within each field. The equation of this line is  $\sigma(A_K) = 0.056(\pm 0.005)\langle A_K \rangle + 0.043(\pm 0.005)$ . This result suggests that the typical apparent angular scale size for an absorbing cloud is small compared with the field size (90'' on a side).

Finally, from an examination of the luminosity function of bright giants in each field we conclude that the young component of the stellar population observed near the Galactic center declines in density much more quickly than the overall bulge population and is undetectable beyond  $1^\circ$  from the Galactic center.

*Subject headings:* Galaxy: abundances — Galaxy: center — Galaxy: stellar content — stars: abundances – color-magnitude diagrams

## 1. Introduction

In a seminal paper, Whitford (1978) demonstrated that the integrated optical light from Baade’s Window in the Galactic bulge ( $b = -4^\circ$ ) closely resembles the light from the bulges of other spirals and from moderate luminosity E and S0 galaxies. Contemporaneous with Whitford’s paper the near-IR (1.2 to 2.2  $\mu\text{m}$ ) light from these galaxies was shown to be dominated by giant stars (Frogel *et al.* 1978). A few years later, Blanco and his collaborators (Blanco *et al.* 1984) established that Baade’s Window contains a high percentage of middle and late M giants compared to the mix of stars in other parts of the Galaxy. Subsequent optical and IR studies of these bulge giants (Frogel 1988; Frogel & Whitford 1987; Frogel *et al.* 1990; Rich 1983; Rich 1988; Terndrup *et al.* 1990, 1991) led to the conclusion that their photometric and spectroscopic properties corresponded to what was expected for the stars inferred to exist in early-type galaxies based on the integrated light observations of the latter. At the same time, these optical and IR studies revealed that the observed luminosities, colors, and spectral characteristics of the bulge stars were significantly different from those of other known M giants.

Nearly all of our present knowledge of stars in the Galactic bulge has been derived from observations of stars in fields with  $|b| \geq 3^\circ$ , i.e. greater than about one scale length. For example, Tiede *et al.* (1995) compiled mean metallicity values for outer bulge fields in order to determine the best estimate for the gradient in metallicity over this region. Minniti *et al.* (1995) discussed the evidence for and meaning of a metallicity gradient in the Galactic bulge but again based on observations of fields exterior to Baade’s Window. For  $|b| \leq 3^\circ$ , on the other hand, reddening and extinction increase strongly so that optical observations become difficult to impossible. Near-IR observations then become the only way that these inner bulge stars can be studied effectively, either photometrically or spectroscopically (e.g., Glass *et al.* 1987; Lebofsky & Rieke 1987; Catchpole *et al.* 1989).

Most of our previous near-IR observations of bulge giants have been in the same fields that have been studied optically. This has allowed us to develop calibrated techniques for estimating key physical parameters for these stars such as reddening, metallicity, and luminosity based on both photometry and low to medium resolution spectroscopy, both in the near-IR. For example, Tiede *et al.* (1995) used the relationship between  $[\text{Fe}/\text{H}]$  and the slope of the upper giant branch (GB) in a  $K, J - K$  color-magnitude diagram (CMD) derived from observations of globular clusters by Kuchinski *et al.* (1995) to estimate the mean metallicity of several fields along the minor axis of the bulge. They found a gradient in  $[\text{Fe}/\text{H}]$  of  $-0.060 \pm 0.033$  dex/degree for the region  $-12^\circ \leq b \leq -3^\circ$ .

If we are to achieve a better understanding of the formation, evolution, and chemical enrichment history of the bulge we must observe stars much closer in to the center. As noted above, these observations are best carried out in the near-IR. The analysis techniques developed with stars in globular clusters and the outer bulge can then be applied to these data. We have already obtained most of the needed  $JHK$  images of selected inner bulge fields. From these data we can calculate stellar luminosities and reddenings, derive luminosity functions, and identify candidate stars for near-IR spectroscopy. We are now in the process of obtaining near-IR spectra and establishing a metallicity calibration for these data from similar observations of giants in metal-rich globular clusters.

The purpose of this paper is to present a preliminary analysis of near-IR CMDs for 11 fields interior to  $-4^\circ$  and as close as  $0.2^\circ$  to the Galactic Center itself. Seven of these fields are on the minor axis; 5 are at a latitude of  $-1.3^\circ$  parallel to the major axis. From these CMDs we first estimate (sections 3.1 and 3.2) the reddening for each field with a technique similar to that employed by Narayanan *et al.* (1996). We then estimate the mean metallicity for each field (section 3.3) using the slope of the giant branch method. This allows us to improve the reliability of our earlier value for the metallicity gradient in the Galactic

bulge (sections 3.4 and 3.5) since our previous data set included only one inner bulge field. While metallicities derived with this technique may not be as accurate as those that can be obtained from spectroscopy, given the impossibility of obtaining “definitive” metallicities from high resolution optical spectroscopy and the relative newness of techniques based on near-IR spectroscopy, application of several different, independent methods to the problem is valuable. Also, we emphasize that although we will refer to metallicity as  $[\text{Fe}/\text{H}]$  in this paper, and we have based our metallicity scale on observations of globular clusters, most of which have had a true Fe abundance determined, the slope of the giant branch could be affected by non-solar abundance ratios with respect to Fe (cf. McWilliam & Rich (1994)) in the bulge. Finally, from a “quick look” at the luminosity functions of the bright giants in each field we are able to address the issue of whether or not there has been a significant amount of continuing star formation in the bulge (section 3.6). In subsequent papers, we will give a detailed analysis of the  $JHK$  colors and luminosities of the giants in these fields and derive independent  $[\text{Fe}/\text{H}]$  estimates from near-IR spectroscopy of the brighter giants in each of the fields.

## 2. Observations and Data Reduction

All of our data were obtained on the 2.5m duPont telescope at Las Campanas Observatory during 1992 and 1993 with IRCAM (Persson *et al.* 1992). The detector was a  $256 \times 256$  HgCdTe NICMOS 3 array with a plate scale of  $0.348 \text{ arcsec pixel}^{-1}$ . The log of the observations is given in Table 1. Figure 1 displays the location of the fields. We have included the location of Baade’s Window in this figure to underscore the fact the new fields provide a good sampling of the entire bulge minor axis interior to Baade’s Window, a region of the Galaxy that, except for the Galactic Center itself, is almost completely unexplored. For the 3 fields closest to the Galactic center (the “c” fields) we chose regions of relatively

uniform extinction based on visual inspection of near-IR images of the immediate vicinity of the Galactic Center (Glass *et al.* 1987), originally presented in Catchpole *et al.* (1985). We note, though, that compared to fields at higher latitudes away from the center, even these fields have very patchy extinction. In all of our logs and data reduction procedures these fields were always referred to as the “Catchpole fields”, hence the “c” designation. The data analyzed in Tiede *et al.* (1995) were obtained as part of this program and the observations were made on the same nights. Data reduction proceeded as described in Tiede *et al.* except for the differences we will now note.

Because we wanted to well sample the upper parts of the GB in each of these fields and because the field of view of IRCAM is small relative to the areas of the higher latitude fields studied by Frogel *et al.* (1990), we imaged one part of each field deeply and then took shorter exposures in a grid pattern, usually  $70''$  on a side. This strategy resulted in the a–d designations in Table 1. The second and third columns of Table 1 give the coordinates of the nominal field centers together with the offsets with respect to these centers of the adjacent fields. For various reasons, the data from the adjacent fields were not always usable, hence the incomplete coverage in Table 1. Usually, there was an overlap region between 10 and  $20''$  for adjacent fields. We caution observers who might use the coordinates in Table 1 that their accuracy is probably not better than  $\pm 10''$ .

The 5<sup>th</sup> and 6<sup>th</sup> columns of Table 1 give the number of images taken and the exposure times. For all pointings, we took 5 images with centers displaced by a few seconds of arc from each other. Short, one second, exposures were always taken to minimize saturation effects on the brightest stars. This series was then immediately followed by a series of 5 longer exposures. If deep exposures were taken on nights judged to be non-photometric, the field was repeated with short exposures on a photometric night. We did not reduce some of our deepest data once we judged that what had been reduced was adequate for this study.

Most of the absolute calibration was based on repeated imaging of two fields in Baade’s Window that contained stars with single channel photometry from Frogel & Whitford (1987). One of these “standard” fields contains stars B20, 28, 31, 36, and 38; the second contains stars B143, 145, 158, 159, 162, 163, and 169. These fields provided calibration for the nights 920714, 920715, and 920718. On 930706 a frame was taken of the globular cluster M5 which contains two stars measured by Frogel *et al.* (1983). For 930707 only a single frame of one of Baade’s Window fields was available for calibration. On these same nights standards from Elias *et al.* (1982) were also observed, but since our main objectives for this preliminary analysis involved relative photometry, we judged the technique just described to be adequate. Stellar photometry in each field was carried out with DoPHOT (Schechter *et al.* 1993), while the calibration transfers were done with the IRAF task qphot. The photometric uncertainties based on scatter in the repeated observations of stars in the standard fields are about 0.04 or 0.05 magnitudes.

### 3. Analysis and Discussion

#### 3.1. Reddening

We determined the average extinction and reddening to each field by assuming that the upper giant branch in each field is similar to the upper giant branch of Baade’s Window (Tiede *et al.* 1995). For Baade’s Window, the upper giant branch is very nearly linear and is defined by those stars with  $8.0 \leq K_0 \leq 12.5$ . The bright cut-off is set to exclude luminous asymptotic giant branch (AGB) stars, while the faint cut-off excludes clump stars. In this magnitude range an analytic expression for the upper giant branch is

$$-0.113(\pm 0.005)K_0 + 2.001(\pm 0.052) = (J - K)_0 \quad (1)$$

where the coefficients and uncertainties were derived by error-weighted least-squares fitting of a line to the data from the Tiede *et al.* dereddened photometry for Baade’s Window. In addition to this equation for the upper giant branch, we used the relation between extinction and reddening found by Mathis (1990)

$$A_K = 0.618E(J - K) \tag{2}$$

to establish the reddening vector in each field.

With Eqns. 1 and 2, we derived an estimate of the average reddening in each subfield by calculating the shift required in  $K$  and  $J - K$  along the reddening vector, to force each star to fall on the Baade’s Window giant branch. Since many of the fields have foreground stars which are located in front of at least some of the reddening, we used an iterative process to exclude these stars from the reddening estimate. The mean and standard deviation were first calculated with all stars in a field. The data was  $2\sigma$ -clipped and the mean and deviation recalculated. Additional iterations did not exclude any additional stars except in the most reddened fields (c2 and c3) which require 4 iterations. This procedure could tend to underestimate the true reddening dispersion in the fields. The final reddening for each subfield (columns 2 and 3 of Table 2) was calculated from the mean of these individual shifts. As can be seen in Table 2, the reddenings derived for each subfield within a given field agree very well. The uncertainties in columns 2 and 3 are based on the star to star scatter in each of the subfields. The averages of the subfield values of  $A_K$  and the dispersion in these averages are given in columns 4 and 5, respectively. In every case these dispersions are smaller than the error in the mean values (col. 6) based on the star to star scatter.

Finally, in addition to the upper and lower magnitude cuts and the sigma-clipping, in the most reddened fields the  $J$  exposures did not go deep enough to sample the entire upper giant branch. This selection effect causes redder stars to be systematically excluded



from the sample for such fields and would result in an artificially low reddening estimate. For these fields we raised the lower magnitude limit up to a level for which there was no selection effect along the upper giant branch. The last column of Table 2 lists the lower  $K$ -magnitude limit used for these fields. Since the upper giant branch is linear in the  $K$ ,  $J - K$  plane, this change in the faint magnitude limit for the upper giant branch does not systematically effect either the reddening estimate or the giant branch slope estimate below (see section 4.2 of Tiede *et al.* 1995 for a discussion).

Representative dereddened CMDs are shown in Figures 2–4. Figure 2 shows CMDs of subfields c1a3 (left panel) and c1b (right panel). The c1 field is at a low latitude and has moderate reddening. The figure illustrates various aspects of our reddening determination procedure. The solid line in both panels is the dereddened upper giant branch from Baade’s Window. The c1 stars have been dereddened by the amount indicated in Table 2. Stars fainter than the dotted line and brighter than the top of the solid line, were excluded for the reasons given above. Stars falling more than  $2\sigma$  from the line in color were excluded primarily to select against foreground stars. In the right panel, stars with  $K_0 > 11.07$  (dotted line) were excluded because the  $J$  frame was not deep enough to give a complete sample unbiased in color. The remaining stars, indicated by filled points, were the ones used to estimate the average reddening in the field. As can be seen in this moderately reddened field, these latter stars, dereddened by the average reddening, fall reasonably well along the upper giant branch defined by the Baade’s Window giants. This morphological agreement with the Baade’s Window giant branch, coupled with the excellent agreements of reddening estimates of different subfields in the same field gives confidence that our method is providing a reasonable estimate of the average reddening.

Figure 3 shows CMDs of subfields c2a (left panel) and c2b (right panel). The c2 field is our most heavily reddened. All of the same exclusions of stars where made as in the

previous example, but note that in this field the lower magnitude limit necessary, due to incompleteness in the  $J$  exposure, is much more extreme, ( $K_0 > 9.49$  for c2a and  $K_0 > 9.41$  for c2b, see dotted lines in Figure 3). However, even in this worse case, the extinction estimates in the two subfields differ only by 0.08 magnitudes in  $K$  (see Table 2). This is only half of the error in the average value. Note that due to the heavy reddening in the c2 field, Figure 3 extends to much brighter magnitudes than either Figure 2 or Figure 4. This is caused by the extinction effectively lowering the saturation to brighter  $K_0$  magnitudes. The number of stars brighter than the tip of the first ascent giant branch is discussed in section 3.6 below.

In contrast, Figure 4 shows CMDs of subfields g0-2.8a (upper left), g0-2.8b (upper right), g0-2.8c (lower left) and g0-2.8d (lower right). Field g0-2.8 has the deepest photometry (b and d subfields) and is typical of all the g field CMDs. Due to the drop-off in stellar density moving away from the Galactic center, the upper giant branches are not as well populated as in the c fields; however, the completeness in the  $J$  exposures at the lower end of the upper giant branch more than makes up for the stars lost due to the density fall-off. Additionally, the decrease in differential reddening in these higher latitude fields, allows a more precise determination of the average reddening.

### 3.2. Differential Reddening

Near the Galactic center, differential reddening due to non-uniform distribution of the intervening dust on small spatial scales makes the study of the stellar population difficult even in the infrared (e.g., Narayanan *et al.* 1996; Davidge 1998). Figure 5 is a plot of  $\langle A_K \rangle$  for each subfield versus the  $1\text{-}\sigma$  scatter about the mean (col. 2 of Table 2) of the individual stars. Since the relative star to star photometric uncertainty is similar for all fields, the difference in scatter from one field to the next is an indicator of true differential reddening

in each field. From this plot, it appears that the amount of differential reddening in a field is directly proportional to the average reddening: the more reddening present in a field, the more patchy that reddening is. A least-squares fit to the points in Fig. 5 (shown by the straight line) is given by;

$$\sigma(A_K) = 0.056(\pm 0.005)\langle A_K \rangle + 0.043(\pm 0.005) \quad (3)$$

where the uncertainties in the coefficients are the formal uncertainties in the fit. The projected scatter at zero extinction, 0.043, is comparable to the typical uncertainty in the photometry, about 0.05 magnitudes.

We searched for a dependence of the difference in reddening between two stars and their spatial separation but found none. This indicates that the typical scale length for significant changes in extinction due to the intervening clouds is comparable to or smaller than a few arc seconds.

### 3.3. Field Metallicities

Kuchinski *et al.* (1995) determined that the slope of the upper giant branch in metal-rich globular clusters is closely correlated with the metallicity of the clusters. Tiede *et al.* (1995) demonstrated that when applied to Baade’s Window giants, this relationship between giant branch slope and metallicity yielded a value for metallicity in agreement with the mean [Fe/H] value determined by McWilliam & Rich (1994) for K giants in Baade’s Window. Tiede *et al.* (1997) recalibrated the relationship for bulge stars and extended it to open clusters. Through this series of papers, the method has been found to be robust to errors in reddening and to be supported by theoretical considerations. We note though that uncertainties in the color transformations between the different detector systems used in the different studies could affect the slope comparisons for fields as heavily reddened as

those discussed here. This is because the change in  $J - K$  color over the part of the giant branch under consideration is about 0.5 magnitudes.

In what follows we will refer to the metallicities we determine as  $[\text{Fe}/\text{H}]$  values although, as pointed out in the Introduction, differences in elemental ratios with respect to iron between bulge fields and globular clusters could affect the values we derive. We derive an estimate of the mean  $[\text{Fe}/\text{H}]$  for each field by allowing the slope of the dereddened giant branch to be a free parameter and then use least-squares to fit a line to the stars selected as upper giant branch stars in section 3.1. Equivalently, we could have determined the slope of the giant branch from the observed colors since *the slope is independent of reddening*, only the intercept will change. However, the reddening calculations described in section 3.1 also indicated likely foreground stars for elimination from the calculations and facilitated choosing a lower limit which excluded clump stars.

The derived  $\langle[\text{Fe}/\text{H}]\rangle$  estimates for each field, the individual mean  $[\text{Fe}/\text{H}]$  values for each subfield, along with the slopes, intercepts and number of selected stars for each subfield are tabulated in Table 3. Some subfields were observed more than once, on different runs or different nights (see Table 1 and Table 2). Only the best exposures were used to calculate mean metallicities. Column 1 of Table 3 indicates these exposures. Fields c2 and c3 were excluded from this analysis because the very large extinction in these fields – both absolute and differential – resulted in a strongly truncated observed giant branch which in turn made both slope determination and foreground-star exclusion excessively uncertain. Fields g4-1.3c,d were excluded because the small total number of stars made it difficult to reliably evaluate foreground contamination.

To calculate  $[\text{Fe}/\text{H}]$  in each subfield we used the relation for bulge stars from Tiede *et al.* (1997):

$$[\text{Fe}/\text{H}] = -1.692(\pm 0.500) - 13.613(\pm 5.118) \times (\text{GB slope}). \quad (4)$$

This recalibration of the relation derived by Kuchinski *et al.* (1995) is based on only 5 minor-axis bulge fields. However, as demonstrated in Figure 2 of Tiede *et al.* (1997), a recalibration of the original metal-rich globular cluster relation is necessary for bulge stars, especially for  $[\text{Fe}/\text{H}] \lesssim -0.4$ .

Columns 5–8 of Table 3 present the results of these calculations. Column 5 lists the  $[\text{Fe}/\text{H}]$  estimates for each subfield calculated from the above relation. Column 6 is the error-weighted average metallicity for each field calculated from the metallicities of each associated subfield. Column 7 is the standard deviation in the subfield metallicity values and column 8 is the formal error propagated through the calibration equations. Most of the standard deviations are not very meaningful since they are each based on only 2 subfields; however, so as not to under estimate the errors in the metallicity values, for subsequent analysis in cases where the standard deviation is larger than the formal error, the standard deviation was used for error analysis.

In theory we could use the newly derived slopes to iterate on our reddening estimates. In practice this will not work since the difference in *true* (as opposed to observed) slopes for each field is actually quite small. If we exclude the fields with the highest reddening and greatest uncertainties in their slopes, c2 and c3, then between  $b = -0.8^\circ$  and  $-2.8^\circ$  the change in average slope is only 0.01. The resulting change in the projection of the reddening vector onto the giant branch will also be small compared with the uncertainties. Thus the derived dispersion in the extinction will not change significantly. Furthermore, since we will still not know the change in the zero point, we could not calculate what the change in reddening would be, although it again would be expected to be small. Although an iterative approach might be expected to work best for the most heavily reddened fields, these also have the most poorly determined slopes due to the relatively small stretch of the giant branch that could be observed in these fields.

### 3.4. Minor-Axis Metallicity Gradient

Tiede *et al.* (1995) published metallicity values derived from the GB slope-metallicity method for minor-axis fields spanning  $-0.2^\circ \leq b \leq -12.5^\circ$ . However, only one field, near the globular cluster Liller 1, fell within 2 degrees of the Galactic center. With our newly derived metallicity values we can, for the first time, determine the minor-axis metallicity gradient for the inner bulge,  $-0.8^\circ \leq b \leq -2.8^\circ$ . We exclude the off-axis fields, g1-1.3, g2-1.3, g3-1.3, and g4-1.3, from consideration in calculating this gradient.

Figure 6 is a plot of derived  $\langle[\text{Fe}/\text{H}]\rangle$  versus galactic latitude,  $b$ , for the inner bulge fields that are close to or on the minor axis. The line is an error-weighted least-squares fit to the points. The slope of the line is  $-0.085 \pm 0.033$  dex/degree with an intercept of  $-0.019 \pm 0.066$  dex. This metallicity gradient agrees with the value found by Tiede *et al.* (1995),  $-0.060 \pm 0.033$ , based primarily on fields at greater Galactocentric distance.

Since there is good agreement between the present determination of the minor-axis metallicity gradient for the inner bulge and that of Tiede *et al.* (1995) for the outer bulge, we combine the two determinations to produce one set of metallicity estimates spanning  $-0.2^\circ \leq b \leq -10.25^\circ$ . The values from Tiede *et al.* (1995) are recalibrated to the new slope-metallicity relation for bulge stars (Eq. 3). The galactic latitudes and  $\langle[\text{Fe}/\text{H}]\rangle$  values are given in Table 4. We exclude the field at  $b = -12.5^\circ$  because, as shown in Tiede *et al.* (1997) (see also Minniti *et al.* 1995), its population is likely dominated by halo/thick disk stars rather than bulge stars. Figure 7 plots the  $\langle[\text{Fe}/\text{H}]\rangle$  estimates from Table 4 versus galactic latitude. The filled circles are data from this study while the open circles are the recalibrated data from Tiede *et al.* (1995). The line is the calculated error-weighted least-squares fit to the 12 points. This fit gives the metallicity gradient for the entire bulge population along the  $b < 0^\circ$  minor-axis to be  $-0.064 \pm 0.012$  dex/degree with an intercept (predicted  $[\text{Fe}/\text{H}]$  value at the Galactic center) of  $+0.034 \pm 0.053$  dex. Values found in

previous studies for the *outer* bulge metallicity gradient are in reasonable agreement with our new value for the entire bulge (see Table 5).

As just noted, our data predict that the bulge population near the Galactic center, presumably the most metal-rich, should have a metallicity value close to solar. This prediction along with the  $\langle[\text{Fe}/\text{H}]\rangle$  values derived along the minor axis are in disagreement with studies such as Blanco *et al.* (1984) and Blanco & Terndrup (1989) which suggested super-solar metallicities based on the large number of M giants present in the bulge, and analyses such as those by Frogel & Whitford (1987), Rich (1988) and Terndrup *et al.* (1990,1991) which also suggested super-solar metallicities for bulge stars in Baade’s Window based on CO index strengths and medium-resolution spectral measurements of the TiO band. However, this prediction is in agreement with later studies such as the high-resolution spectroscopy of K giants in Baade’s Window by McWilliam & Rich (1994) and the conclusion by Houdashelt (1995) that the stars in the Galactic bulge are more similar to the sub-solar metallicity stars found in lower-mass elliptical galaxies than the super-solar metallicity stars found in massive elliptical galaxies. This evidence suggests that bulge stars are selectively enriched in certain elements (e.g., Ti and O) while their overall metallicities, as measured by the GB slope - metallicity relation (cf. Tiede *et al.* 1995), are just below solar.

Most previous photometric and spectroscopic studies, both in the red and near-IR, of the M giants in the Galactic bulge have not given a hint of a spread in metallicity at any given latitude, particularly in Baade’s Window (e.g. Frogel & Whitford (1987), Terndrup *et al.* 1990, 1991). In contrast, high resolution optical studies of K giants in Baade’s Window (e.g. Rich 1988) show the existence of a spread in  $[\text{Fe}/\text{H}]$  of nearly a factor of 100. With the new data presented here it would be difficult to distinguish a spread in metallicity from dispersion of reddening. Nevertheless, the fact that the dispersion in  $(J - K)$  is about 0.10

mags or less for many of the fields we have surveyed, suggests that a metallicity dispersion approaching a factor of 100 would not be allowed by our new data for the inner bulge. Based on observations of globular cluster giant branches and of fields in the outer bulge, we estimate that the allowable range in metallicity dispersion for a give field is likely to be no more than a factor of 10 (Frogel *et al.* 1990).

Measuring the  $\langle[\text{Fe}/\text{H}]\rangle$  of the bulge population at the Galactic center is problematic due to the extremely high reddening and reddening dispersion as demonstrated, for example, by Blum *et al.* (1996a) and Narayanan *et al.* (1996). Additionally, Blum *et al.* (1996b) have shown that the Galactic center region contains stars from distinct star-formation epochs with ages from  $\sim 7$  Myrs (the most recent) to  $\sim 10$  Gyrs (the bulge population). However, Ramírez *et al.* (1997) have begun to measure metallicities for Galactic center stars based on high-resolution spectral analysis and determine a  $\langle[\text{Fe}/\text{H}]\rangle$  value (based on measurements of actual Fe absorption lines) of  $-0.07 \pm 0.11$  for 10 stars of various ages, including 2 which are super giants and so belong to the youngest epoch of star formation. It appears that while the bulge may have enriched faster than the halo or disk, even the most recent epoch of star formation in the Galactic center did not produce an easily detectable population of super-solar metallicity stars.

We conclude this subsection by noting the following: The medium and high resolution optical spectroscopy for Baade’s Window K giants as well as similar data for higher latitude fields probably give the most reliable indicators of stellar abundances in the outer bulge. Therefore, there is considerable need to understand why most of the analyses of the M giants, both optically and in the near-IR have yielded findings at odds with the K giant studies, in particular the mean value for  $[\text{Fe}/\text{H}]$  and its dispersion. Resolution of these conflicting results is especially important because of the fact that only near-IR data can be obtained for much of the inner bulge.



### 3.5. Major-Axis Metallicity Gradient

With the increasing complexity of kinematic models of the inner galaxy and bulge, it is not obvious whether a major-axis metallicity gradient is expected or not. With the asymmetric kinematics suggested by models such as Zhao (1996), line-of-sight distributions of stars may peak in density at different Galactocentric radial distances complicating the projected composite population seen at particular  $(\ell, b)$ . To investigate this matter, we plot  $\langle[\text{Fe}/\text{H}]\rangle$  versus galactic longitude of our 5 fields with  $b = -1.3$ , in Figure 8. The line is an error-weighted least-squares fit to the points. The data only span the inner  $4^\circ$  of longitude in the first Galactic quadrant, however, we find no evidence for a metallicity gradient; the slope of the line is  $0.004 \pm 0.080$  dex/degree.

### 3.6. Young Population in the Inner Bulge

While many studies have now identified bright, young super giants and luminous AGB stars in the region within a few arc minutes of the Galactic center (e.g., Blum *et al.* 1996a,b; Narayanan *et al.* 1996), none have made a study of the extent of the spatial distribution of these stars in the inner bulge. Our inner fields; c1, c2, and c3, have a large number of stars brighter than the giant branch tip (for  $R_0 = 8.0$  Kpc,  $K_0 \sim 8.0$ ). While some of these bright stars are bulge asymptotic giant branch stars or foreground giants, the large number suggests that many could be members of a young population.

Since our various fields have different areas and are complete to different  $K_0$ , we examined the distribution of these bright stars by calculating the ratio of the number of stars with  $K_0 < 8.0$ , including all saturated stars, to the number of old bulge population upper giant branch stars with  $K_0$  magnitudes in the range  $8.0 \leq K_0 \leq 9.4$ . The 9.4 magnitude faint limit was selected so that all of our fields would be complete in this range.

The calculated ratios along with the angular radial distance from the Galactic center are tabulated in Table 6 and displayed in Figure 9.

Table 6 lists each field, Galactic coordinates of the center of each field, the angular radial distance from the Galactic center, the number of stars in each  $K_0$  magnitude range, and the ratio of the number of bright stars to the number of faint stars. The error associated with each ratio is the formal counting error propagated through the ratio. Figure 9 is a plot of these ratios versus angular distance from the Galactic center. The solid points are the minor-axis fields. The open squares are the major-axis fields. The solid square is field g0-1.3 where the major- and minor-axis field groups intersect. The  $\otimes$  is the ratio for Baade’s Window from the luminosity function presented in Tiede *et al.* (1995).

While the uncertainties in individual ratios are generally quite large, we note two trends. Along the minor axis (solid points) the ratio decreases from  $\sim 0.6$  for the inner most fields to  $\sim 0.3$  for the g0-1.3 field,  $1.3^\circ$  from the Galactic center. At radial distances greater than  $1.3^\circ$ , the ratio remains generally constant around 0.3 for both the minor-axis fields and the fields which parallel the major axis. In fact, the average value for all of these fields is about 0.3. The horizontal line in Figure 9 is drawn at this value. This is also the value found in Baade’s Window (the circled “x” in Fig. 9) which is not known to contain any luminous, young stars (DePoy *et al.* 1993; Blum *et al.* 1996a). Therefore, it seems likely that the young population is confined to within  $\sim 1^\circ$  of the Galactic center and bright stars outside this region are old bulge population asymptotic giant branch stars.

Finally, we note that the presence of a significant number of relatively young AGB stars in the two innermost “c” fields (c2 and c3) could contribute to the scatter in the CMDs for these fields. However, based on observations of clusters with a wide range in age in the Large Magellanic Cloud (Frogel, Mould, & Blanco 1990), the expected scatter in  $(J - K)_0$  due to a wide age spread is about 0.1 mags, less than half of that observed in c2

and c3 (Fig. 3 and Table 2).

#### 4. Conclusions

In this work we analyze near-IR,  $JK$ , photometry for 11 fields in the inner  $4^\circ$  of the Galactic bulge. Seven of these fields are along the minor axis spanning from  $b = -2.8^\circ$  to  $-0.2^\circ$ . The other fields are arranged parallel to the major axis at  $b = -1.3^\circ$ .

We determined the average extinction and reddening in each field by assuming the old bulge population present in each window has an upper giant branch similar to that found in  $K, J - K$  color magnitude diagrams of Baade’s Window. We constructed  $K, J - K$  CMDs for each field and calculated the average shift along the reddening vector required for the giant branch to coincide with the Baade’s Window giant branch. The resulting extinctions, displayed in Table 2, ranged from  $E(J - K) = 0.27 \pm 0.05$  to  $2.15 \pm 0.16$ .

We found that the dispersion in  $K$  and  $J - K$  around each giant branch is larger than can be accounted for by photometric uncertainty and that the size of this dispersion is directly proportional to the average extinction in the field. Thus, differential reddening seems to directly correlate with increased extinction in the fields.

Using the reddening estimates to exclude likely foreground and clump stars, we derived an estimate of the  $\langle[\text{Fe}/\text{H}]\rangle$  for each field using the correlation between the slope of the upper giant branch and  $[\text{Fe}/\text{H}]$  derived by Kuchinski *et al.* (1995) and recalibrated for bulge stars by Tiede *et al.* (1997). With the exception of the fields with large differential reddening for which the method is unreliable, we found  $\langle[\text{Fe}/\text{H}]\rangle$  to generally be just below solar,  $\langle[\text{Fe}/\text{H}]\rangle \sim -0.2$ .

We derived the gradient in mean metallicity along the minor axis of the inner Galactic bulge in the range  $-0.2^\circ \geq b \geq -2.8^\circ$ . This result was combined with that of Tiede *et al.*

(1995) based almost completely on data for fields exterior to the present ones, extending to  $b = -10.25^\circ$ , and derived a metallicity gradient for the entire bulge minor axis. This gradient is  $-0.064 \pm 0.012$  dex/degree with an intercept (predicted value of  $[\text{Fe}/\text{H}]$  at the Galactic center) of  $+0.034 \pm 0.053$  dex. This near-solar value for the Galactic center agrees with the recently determined value for  $\langle [\text{Fe}/\text{H}] \rangle$  for the bright stars in the Galactic center based on high resolution near-IR spectroscopy. We also examined 5 fields distributed in galactic longitude but along a line of constant latitude of  $b = -1.3^\circ$ , and found no evidence of a major-axis metallicity gradient.

Finally, we observed that there were a significant number of stars brighter than the giant branch tip (for  $R_0 = 8.0$  Kpc,  $K_0 \approx 8.0$ ) in our inner most fields, but fewer in the more distant fields. To examine the distribution of these bright stars, we calculated the ratio of the number of stars with  $K_0 < 8.0$  to the number of stars with  $8.0 \leq K_0 \leq 9.4$ . We found that the ratio quickly drops from  $\sim 0.6$  in the inner most fields to  $\sim 0.3$  in the field  $1.3^\circ$  from the Galactic center. This 0.3 value is generally characteristic for all fields further from the Galactic center, including Baade’s Window which is known to contain no bright young stars like those found at the Galactic center. Thus we conclude that the young Galactic center population does not extend out beyond  $1^\circ$  from the Galactic center. Beyond this distance, stars brighter than the giant branch tip are likely asymptotic giant branch stars associated with the old bulge population.

We thank Kris Sellgren, Solange Ramírez, and Don Terndrup for helpful comments and discussion. JAF thanks Leonard Searle for the observing opportunities provided by a Visiting Research Associateship at LCO where the data were obtained. This research was supported in part by NSF grant AST92-18281 to JAF. We are particularly grateful to S. E. Persson for the use of IRCAM (built with NSF funds) at LCO and also thank Miguel Roth, Bill Kunkel, and members of the LCO support crew for their able assistance in the

set up and operation of IRCAM and the duPont telescope. We appreciate the advice given by Paul Schechter on the use of DoPHOT which was developed with the aid of NSF grant AST83-18504.

## REFERENCES

- Blanco, V. M., McCarthy, M. F., & Blanco, B. M. 1984, AJ, 89, 636
- Blanco, V. M., & Terndrup, D. M. 1989, AJ, 98, 843
- Blum, R. D., Sellgren, K., & DePoy, D. L. 1996, ApJ, 470, 864
- Blum, R. D., Sellgren, K., & DePoy, D., L. 1996, AJ, 112, 1988
- Catchpole, R. M., Glass, I. S., & Whitelock, P. A. 1989, IAUS, 136, 75
- Catchpole, R. M., Whitelock, P. A., & Glass, I. S. 1985, *The Milky Way Galaxy*, eds. van Woerden, H. *et al.*, Reidel, Dordrecht, Holland
- Davidge, T. J. 1998, AJ, 115, 2374
- Elias, J. H., Frogel, J. A., Matthews, K., & Neugebauer, G. 1982, AJ, 87, 1029
- Frogel, J. A. 1988, ARA&A, 26, 51
- Frogel, J. A., Mould, J. R., & Blanco, V. M. 1990, ApH, 352, 96
- Frogel, J. A., Persson, S. E., Aaronson, M., & Matthews, K. 1978, ApJ, 220, 75
- Frogel, J.A., Persson, S. E., & Cohen, J. G. 1983, ApJS, 53, 713
- Frogel, J. A., Terndrup, D. M., Blanco, V. M., & Whitford, A. E. 1990, ApJ, 353, 494
- Frogel, J. A., & Whitford A. E. 1987, ApJ, 320, 199
- Glass, I. S., Catchpole, R. M., & Whitelock, P. A. 1987, MNRAS, 227, 373
- Houdashelt, M. 1995 thesis, The Ohio State University
- Kuchinski, L. E., Frogel, J. A., Terndrup, D. M., & Persson, S. E. 1995, AJ, 109, 1131

- Lebofsky, M. J. & Rieke, G. H. 1987, in AIP Conference Proceedings, No. 155, The Galactic Center, ed. D. C. Backer, p. 79
- Mathis, J. S. 1990, ARA&A, 28, 37.
- McWilliam, A., & Rich, R. M. 1994, ApJS, 91, 749
- Minniti, D., Olszewski, E. W., Liebert, J., White, S. D. M., Hill, J M., & Irwin, M.J. 1995, MNRAS, 277, 1293
- Narayanan, V. K., Gould, A., & DePoy, D. L. 1996, ApJ, 472, 183
- Persson, S. E., West, S. C., Carr, D. M., Sivarahakrishnan, A, & Murphy, D. C. 1992, PASP, 104, 204
- Ramírez, S. V., Sellgren, K., Carr, J. S., Balachandran, S., Blum, R., & Terndrup D. M. 1997, Proc. of the IAU Symp. 184, The Central Regions of the Galaxy and Galaxies, Kyoto, Japan
- Rich, R. M. 1983 Ph.D. thesis, UCSC
- Rich, R. M. 1988, AJ, 95, 828
- Schechter, P. L., Mateo, M, & Saha, A. 1993, PASP, 105, 1342
- Terndrup, D. M. 1988, AJ, 96, 884
- Terndrup, D. M., Frogel, J. A., & Whitford, A. E. 1990, ApJ, 357, 453
- Terndrup, D. M., Frogel, J. A., & Whitford, A. E. 1991, ApJ, 378, 742
- Tiede, G. P., Frogel, J. A., & Terndrup, D. M. 1995, AJ, 110, 2788
- Tiede, G. P., Martini, P., & Frogel, J. A. 1997, AJ, 114, 694

Tyson, N. D. 1991, Ph.D. thesis, Columbia University

Whitford, A. E. 1978, ApJ, 226, 777

Zhao, H. 1996, MNRAS, 283, 149



Fig. 1.— Galactic positions of our 11 fields. The dotted lines represent the major and minor Galactic Axes. The location of Baade’s Window is shown for reference.

Fig. 2.—  $K_0, (J - K)_0$  color magnitude diagrams of two of the subfields from our c1 field; this is our lowest latitude field on the minor axis. It has moderate reddening,  $E(J - K) = 1.67 \pm 0.15$ . The solid line is the dereddened giant branch from Baade’s Window, used to estimate reddening. The dotted horizontal line is the completeness limit in the  $J$  frame. The open points were excluded from the reddening determination (see text for details).

Fig. 3.—  $K_0, (J - K)_0$  color magnitude diagrams of two of the subfields from our c2 field. Field c2 is the most heavily reddened field in our data and contains a large number of stars brighter than the giant branch tip. Lines and points are the same as in Figure 2.

Fig. 4.—  $K_0, (J - K)_0$  color magnitude diagrams of the four subfields from our g0-2.8 field. g0-2.8 is typical of all the g field CMDs. The b and d subfields have deeper photometry than the a and c subfields. The small number of stars along the upper giant branch relative to the c fields is due to decreased stellar density at larger galactic latitudes. Lines and points are the same as in Figure 2.

Fig. 5.— Mean extinction at  $K$  versus the  $1-\sigma$  scatter about the mean for our subfields. Note that the scatter in  $A_K$  is directly proportional to  $A_K$  in these fields. The line is a least-squares fit to the data.

Fig. 6.— Mean field metallicity versus Galactic latitude in degrees along the minor-axis for our minor-axis fields. Data are from Table 4. The line is an error-weighted least-squares fit to the points. The slope of the line is  $-0.085 \pm 0.033$  dex/degree.

Fig. 7.— Mean field metallicity versus Galactic latitude in degrees along the minor-axis for our minor-axis fields (open circles) and fields from Tiede *et al.* (1995) (solid circles). The [Fe/H] values from Tiede *et al.* (1995) have been recalibrated to the Tiede *et al.* (1997) system (see Table 4) to be consistent with the values for our fields. The line is an error-weighted least-squares fit to all of the data. The slope of the line is  $-0.064 \pm 0.012$  dex/degree with an intercept of  $+0.034 \pm 0.053$  dex.

Fig. 8.— Mean field metallicity versus Galactic longitude in degrees for our fields distributed parallel to the major axis at  $b = -1.3^\circ$ . The line is an error-weighted least-squares fit to the data. The slope of the line is  $0.004 \pm 0.080$  dex/degree, consistent with no metallicity gradient in Galactic longitude.

Fig. 9.— The ratio of the number of stars with  $K_0 < 8.0$  to the number of stars with  $8.0 \leq K_0 \leq 9.4$  versus Galactocentric distance in degrees. Solid points are the minor-axis fields. The open squares are the major-axis fields. The solid square is field g0-1.3 where the major- and minor-axis field groups intersect. The  $\otimes$  is the ratio for Baade’s Window calculated from the luminosity function presented in Tiede *et al.* (1995). The average for all fields with Galactocentric distances greater than 1 degree is nearly equal to the Baade’s Window value and is represented by the horizontal line in the figure.